

Phase separation of co-evaporated ZnPc:C

メタデータ	言語: eng 出版者: 公開日: 2017-10-03 キーワード (Ja): キーワード (En): 作成者: メールアドレス: 所属:
URL	https://doi.org/10.24517/00010544

This work is licensed under a Creative Commons Attribution-NonCommercial-ShareAlike 3.0 International License.



Phase separation of co-evaporated ZnPc:C₆₀ blend film for highly-efficient organic photovoltaics

Ying Zhou^{1,a)}, Tetsuya Taima^{1,2,b)}, Tetsuhiko Miyadera^{2,3}, Toshihiro Yamanari³, Michinori Kitamura,⁴
Kazuhiro Nakatsu,⁴ Yuji Yoshida³

¹Research Center of Sustainable Energy and Technology, Kanazawa University, Kakuma, Kanazawa, Japan

²JST-PRESTO, Japan Science and Technology Agency (JST), 4-1-8 Honcho Kawaguchi, Saitama, Japan

³Research Center for Photovoltaic Technologies, National Institute of Advanced Industrial Science and Technology (AIST), AIST Tsukuba Central 5, 1-1-1 Higashi, Tsukuba, Japan

⁴Sumika Chemical Analysis Service, Ltd., Tsukuba 300-3266 Japan

Abstract

We demonstrate phase separation of co-evaporated zinc phthalocyanine (ZnPc) and fullerene (C₆₀) for efficient organic photovoltaic cells. With introducing a poly(3,4-ethylenedioxythiophene):poly(styrene sulfonate) film and a crystalline copper iodide film on indium tin oxide, 20-nm-thick ZnPc film adopt a lying-down crystalline geometry with grain sizes of about 50 nm. This surface distributed with strong interaction areas and weak interaction areas enables the selective growth of ZnPc and C₆₀ molecules during following co-evaporation, which not only results in a phase separation, but also improve the crystalline growth of C₆₀. This blend film greatly enhances the efficiencies in photocurrent generation and carrier transport, resulting in a high power conversion efficiency of 4.56% under 1 sun.

In recent years, significant progress towards commercialization has been achieved in organic photovoltaics (OPVs), since the introduction of donor-acceptor interface.^{1,2} The highest power conversion efficiency (PCE) reported in single heterojunction reaches 8-10% in solution-processed

^{a)} Electronic mail: zhou@se.kanazawa-u.ac.jp, ^{b)} Electronic mail: taima@se.kanazawa-u.ac.jp

bulk heterojunction (BHJ) OPV cells, which utilize a blend of polymer and acceptor.^{3,4} After thermally annealing the mixture of long-chain polymers and [6,6]-phenyl-C₆₁-butyric acid methyl ester (PCBM), self-assembly of polymers leads to a phase separation in the blend film, resulting in a nanoscale interpenetrating network morphology.^{5,6} Such BHJ not only provides large interface area for exciton dissociation into free charge carriers, but also provides continuous pathways for charge carrier transport. Similar phase separation has been also reported in soluble small molecules.⁷ Furthermore, developing new organic donors with strong intermolecular interaction can enhance the crystalline order in both of donor and PCBM.^{8,9} On the other hand, vacuum evaporation enables better thickness control, thus it is suitable for fabricating tandem (multi-junction) OPV cell, which has also achieved promising performances.^{10,11} However, for vacuum evaporation, it remains challenge to directly control the morphology and crystalline order of co-evaporated blend film, possibly because most of molecular donors (i.e. phthalocyanine) used to date show similar size and intermolecular interaction to fullerene (C₆₀). Many efforts have been made to optimize the blend films. For example, with heating the substrate, varying the evaporation ratio, introducing buffer layers during deposition, PCEs has been greatly improved.¹²⁻¹⁸ Apparently, there is still a lot of room for the improvement of small molecule OPV cell, if phase-separated blend film being comparable with polymer BHJ can be achieved by vacuum evaporation.

In this paper, we demonstrate an efficient approach to realize the phase separation in co-evaporated blend film by patterning the substrate with nanostructured lying-down crystalline zinc phthalocyanine (ZnPc). In order to modify the surface of indium-tin-oxide (ITO) substrate, poly(3,4-ethylenedioxythiophene):poly(styrene sulfonate) (PEDOT:PSS) and copper iodide (CuI) thin films were prepared, respectively. It has been reported that the strong interfacial coupling between surface electronic states of CuI and π -orbitals of molecules leads to a lying-down molecular geometry, which greatly enhanced the OPV cell performances.¹⁹ Here, we show that further morphological and crystalline modifications on ZnPc thin film influence the following growth of ZnPc and C₆₀ molecules during the co-evaporation, resulting in phase separation morphology. With this promising architecture, the OPV cell exhibits a very high PCE of 4.56% under 1 sun illumination (100 mW/cm²).

40-nm-thick PEDOT:PSS film was spin-coated on ITO, and annealed at 135 °C for 30 min with a hotplate. Then, CuI film with a thickness of 5 nm was evaporated. The cell contains typical p-i-n structure by evaporating ZnPc (20 nm), ZnPc:C₆₀ blend (40 nm) and C₆₀ (40 nm) films at room temperature (around 25°C), respectively. Finally, 8-nm-thick bathocuproine (BCP) and 100-nm-thick Al films were deposited as a hole block layer and an electrode, respectively. For reference, OPV cells using same process for growing active layers were also fabricated on bare ITO, ITO/PEDOT:PSS and ITO/CuI, respectively. The cells were measured under simulated AM 1.5 G solar illumination with a Keithley 2400 Digital Source Meter. Incident power was calibrated by using a standard silicon photovoltaic to match 1-sun intensity (100 mW/cm²). Incident photon-to-electron conversion efficiency (IPCE) curves were collected using a xenon lamp, integrated with a computer controlled monochromator. Transmission electron microscopy (TEM), atomic force microscopy (AFM) and X-ray diffraction (XRD) were used to investigate the growth characteristics of organic films.

Figure 1 shows the schematic energy level diagram of the OPV cell with CuI.^{19,20} Figure 2 shows the current-density versus voltage (*J-V*) characteristics and IPCE spectra of the OPV cells and Table I summarizes the main parameters. Compared with the typical cell fabricated on bare ITO (or ITO/PEDOT:PSS), the cell fabricated on ITO/CuI shows a slight increase in short-circuit current from 9.68 (or 9.01) to 10.3 mA/cm², and a significant increase in fill factor (FF) from 0.46 (or 0.32) to 0.59, which results in a 30% increase in PCE (3.19%). The IPCE shows the wavelength dependence of *J*_{SC}, where the peaks centered at wavelengths of $\lambda=630$ and $\lambda=700$ nm correspond to ZnPc absorption and the peak centered at $\lambda=450$ nm corresponds to C₆₀ absorption. IPCE [see Fig. 2(b)] in ZnPc absorption region is increased with introducing CuI thin film due to improved light absorption efficiencies in lying-down ZnPc molecules, while these cells show close photocurrent-generation efficiencies in C₆₀ absorption region. It indicates that similar ZnPc:C₆₀ blend layers were formed. Note that the combination of PEDOT:PSS and CuI films results in a further 50% increase in *J*_{SC} from 10.3 to 15.1 mA/cm². This increase results from the improved efficiencies of photocurrent generation in both of ZnPc and C₆₀ absorption regions, where the IPCE spectra are increased from 29.4% to 40.6% at $\lambda=450$ nm and from 46.1% to 62.4% at $\lambda=630$ nm, respectively. Compared with the cell prepared on

ITO/PEDOT:PSS, the significant improvements in J_{SC} and FF results in a three-fold increase in PCE from 1.55% to 4.56%.

It has been reported that CuI film enables the growth of lying-down ZnPc molecules.¹⁹ As shown in Fig. 1, CuI thin film not only raises the work function of ITO, but also prevents the electrons in active layer from traveling to ITO. Photoemission spectra indicate that CuI thin films evaporated on single crystalline and poly crystalline TiO₂ surfaces have similar band structures.²¹ Inserting CuI thin film can greatly improve the efficiencies in light absorption, charge transport as well as charge collection. There are another two possible reasons should be considered for the further improvements with a combination of PEDOT:PSS/CuI: (1) exciton confinement effect²² resulting from CuI thin film; (2) morphological variations in BHJ. Because ZnPc exhibits weak photoluminescence (PL) quantum efficiency, boron subphthalocyanine chloride (SubPc) thin films were deposited to investigate the exciton confinement effect of CuI. However, the similar PL spectra of SubPc films indicate that CuI thin film has limited exciton confinement effect. Thus, BHJ morphology plays a key role in further improvements of cell performances.

To better understand the relationships between BHJ morphology and cell performances, the actual cells were investigated by TEM. Figure 3(a) shows a cross-sectional bright field (BF) TEM image of the cell fabricated on ITO/PEDOT:PSS (PCE=1.55%). Some crystallites with an average diameter of 20 nm are observed, while the image contrast is not high enough to recognize the layered cell structure. On the other hand, energy filtered (EF) TEM provides an image contrast based on the difference in electron energy loss spectrum (EELS) of materials in plasmon region.²³⁻²⁵ The cell structure can be identified when energy loss at 28 eV is introduced for EFTEM imaging, as shown in Fig. 3(b). For photoactive layers, relatively darker area corresponds to ZnPc while brighter area corresponds to C₆₀, because the inelastic scattering (plasmon scattering) from C₆₀ is more intense at 28 eV according to the EELS spectra of C₆₀ and ZnPc (not shown here). Between ZnPc and C₆₀ films, the ZnPc:C₆₀ blend film with a moderate color contrast is also observed. Note that no clear structures can be recognized in this uniform film. It implies that the domains of ZnPc or C₆₀ are too small to be resolved, and that phase separation does not occur. It is well known that the blend film provides large interface area for exciton dissociation, which always leads to a high J_{SC} . However, these small isolated domains of ZnPc or C₆₀

result in many trap sites inside the blend film, which greatly degrade the efficiency in charge carrier transport due to the recombination. Therefore, the cell fabricated on ITO/PEDOT:PSS shows a very poor FF of 0.32. Fig. 3(c) and 3(d) show the BFTEM and EFTEM images of the cell fabricated on ITO/PEDOT:PSS/CuI (PCE=4.56%). The layered cell structure with a PEDOT:PSS film and a high-quality crystalline CuI film is observed. Note that the blend film exhibits an interpenetrating network with phase-separated ZnPc and C₆₀ domains. Interestingly, the sizes of ZnPc and C₆₀ domains are both about 20 nm, which are within the exciton diffusion lengths of ZnPc (10-40 nm)^{26,27} and C₆₀ (10-20 nm).^{28,29} Excitons generated in blend film (both of ZnPc and C₆₀ domains) can efficiently diffuse into the dissociation sites. It is consistent with the improved IPCE spectra in both C₆₀ and ZnPc absorption regions [Fig. 2(b)]. Moreover, C₆₀ crystallites are identified not only in the pure C₆₀ film but also in the blend film, as shown in large-scale images [Fig. 3(e)]. These continuous pathways with high-quality crystalline order significantly improve the charge carrier transfer efficiency, resulting in an 80% increase in FF from 0.32 to 0.59. We also fabricated a reference cell utilizing only 20 nm blend film, which exhibits a high PCE of 4.37% (Table I).

The phase separation during co-evaporation is attributed to the structural characteristics of pre-deposited pure 20-nm-thick ZnPc film. Figure 4 shows the height-contrast and phase-contrast AFM images of ZnPc films. Apparently, the growth of ZnPc films strongly depends on the substrates. On ITO/CuI, ZnPc film shows a very smooth surface morphology, and crystal-like structures cannot be identified in both height and phase images [Fig. 4(a) and 4(d)]. When the rough ITO surface was smoothed by a spin-coated PEDOT:PSS film, ZnPc molecules can diffuse a longer distance to grow larger island, resulting in the formation of fiber-like grains, as shown in Fig 4(b). Moreover, the phase image in Fig. 4(e) indicates that most of the fiber-like grains connect with each other, and on the whole a uniform surface morphology is formed. On the other hand, after deposition of a crystalline CuI film on ITO/PEDOT:PSS, ZnPc shows three-dimensioned round grains with an average diameter of about 50 nm [Fig. 4(c)]. Since the phase image (phase lag) is sensitive to the variations in materials properties such as adhesion and viscoelasticity, the large phase contrast between grain and boundary [Fig. 4(f)] indicates that these isolated grains show very different characteristics. Figure 5 shows the X-ray diffraction (XRD) spectra of ZnPc films. The diffraction peaks centered at $2\theta=6.9^\circ$ and $2\theta=27.8^\circ$

correspond to the standing-up ZnPc crystalline order (S-ZnPc, $d=12.9$ Å) and lying-down ZnPc crystalline order (L-ZnPc, $d=3.2$ Å), respectively. ZnPc grown on bare ITO shows a very weak diffraction peaks at $2\theta=6.9^\circ$. The standing-up crystalline order of ZnPc is significantly enhanced when PEDOT:PSS was pre-prepared on ITO. Moreover, amorphous ZnPc film is formed on ITO/CuI, which has a good agreement with AFM results. Note that pre-prepared PEDOT:PSS also enhance the crystalline growth of CuI, which results in a lying-down crystalline ZnPc geometry. The results indicate that the grains observed in Fig. 4(c) are ZnPc crystalline domains.

Generally, for π -conjugated molecules, the molecule-substrate interfacial interaction and intermolecular interaction dominate the film growth,³⁰ which includes absorption/desorption, nucleation, surface diffusion and island (crystal) growth. Especially, for planar π -plane molecules like ZnPc, controlling the crystalline orientation in order to obtain lying-down (π - π) geometry has been widely investigated for pure ZnPc layer,³¹⁻³⁴ i.e. introducing a CuI film which exhibits a strong interaction with molecules.¹⁹ We believe that these interactions also play an important role in the growth of blend film during co-evaporation. Because ZnPc-ZnPc (standing-up) and C_{60} - C_{60} exhibit large intermolecular distances of about 13 Å, they have similarly weak intermolecular interactions and abilities for diffusion during the film growth. On the surface of standing-up ZnPc, van der Waals force (weak interaction) dominates the nucleation and growth of both ZnPc and C_{60} molecules. The randomly absorbed ZnPc and C_{60} molecules will prefer to form nucleation sites on each other, rather than diffuse a long distance to grow large domains. Uniform blend film [Fig. 3(b)] is usually formed under normal co-evaporation conditions. To break this thermodynamic equilibrium state during co-evaporation in order to grow large domains, heating the substrate and varying materials ratio are possible approaches.¹²⁻¹⁸ These approaches require very careful handling, and it still remains difficulties for preparing an interpenetrating network (morphological control on both molecules). On the other hand, π - π stacking ZnPc molecules exhibit significantly stronger intermolecular interaction compared with van der Waals force. It seems that the patterned surface with nanostructured ZnPc is distributed with strong interaction areas (lying-down ZnPc grains) and weak interaction areas (grain boundaries), as shown in Fig. 4(c) and 4(f). It is inferred that more ZnPc molecules are absorbed on the ZnPc grains to form nucleation sites. The strong interaction also enables more ZnPc molecules

diffuse to grow large domains. Correspondingly, more C₆₀ molecules have to form nucleation sites at the grain boundaries, where van der Waal force plays a role. Moreover, without influences from neighboring ZnPc molecules, C₆₀ molecules have more freedom to grow crystallites as in pure C₆₀ film. Thus, constructing a nanostructured surface to enable the selective growth of co-evaporated molecules is crucial for this interesting self-assembly phase separation.

In summary, we demonstrate an attractive approach to realize self-assembly phase-separation by vacuum evaporation, which forms ideal BHJ for highly-efficient small molecule OPV. By smoothening ITO surface with PEDOT:PSS, a high-quality crystalline CuI thin film is formed, which results in a nanostructured ZnPc surface morphology with lying-down crystalline order. This surface distributed with strong interaction areas and weak interaction areas enables the selective growth of ZnPc and C₆₀ molecules during co-evaporation. The TEM analysis on cell structure indicates that this selective growth not only results in phase separation, but also improves the crystalline growth of C₆₀ in the blend film. With the promising BHJ structure, the OPV cell utilizing ZnPc/C₆₀ exhibits a high PCE of 4.56% under 1 sun illumination.

This work was supported by the Precursory Research for Embryonic Science and Technology (PRESTO) program from the Japan Science and Technology Agency (JST).

¹C. W. Tang, *Appl. Phys. Lett.* **48**, 183 (1986).

²S. Sista, Z. Hong, L. M. Chen, and Y. Yang, *Energy Environ. Sci.* **4**, 1606 (2011).

³G. Li, R. Zhu, and Y. Yang, *Nat. Photonics*, **6**, 153 (2012).

⁴M. A. Green, K. Emery, Y. Hishikawa, W. Warta, and E. D. Dulong, *Prog. Photovolt: Res. Appl.*, **20**, 12 (2012).

⁵C. J. Brabec, M. Heeney, I. McCulloch, and J. Nelson, *Chem. Soc. Rev.* **40**, 1185 (2011).

⁶A. Facchetti, *Chem. Mater.* **23**, 733 (2011).

⁷B. Walker, C. Kim, and T. Q. Nguyen, *Chem. Mater.* **23**, 470 (2011).

⁸I. Osaka, M. Saito, H. Mori, T. Koganezawa, and K. Takimiya, *Adv. Mater.* **24**, 425 (2012).

⁹Y. Sun, G. C. Welch, W. L. Leong, C. J. Takacs, G. C. Bazan, and A. J. Heeger, *Nat. Mater.* **6**, 1 (2011).

- ¹⁰M. Riede, C. Urich, J. Widmer, R. Timmreck, D. Wynands, G. Schwartz, W. M. Gnehr, D. Hildebrandt, A. Weiss, J. Hwang, S. Sundarraj, P. Erk, M. Pfeiffer, and K. Leo, *Adv. Funct. Mater.* **21**, 3019 (2011).
- ¹¹J. Meiss, T. Menke, K. Leo, C. Urich, W. M. Gnehr, S. Sonntag, M. Pfeiffer, and M. Riede, *Appl. Phys. Lett.* **99**, 043301 (2011).
- ¹²S. Pfuetzner, J. Meiss, A. Petrich, M. Riede, and K. Leo, *Appl. Phys. Lett.* **94**, 253303 (2009).
- ¹³T. Osasa, S. Yamamoto, and M. Matsumura, *Adv. Funct. Mater.* **17**, 2937 (2007).
- ¹⁴S. Pfuetzner, C. Mickel, J. Jankowski, M. Hein, J. Meiss, C. Schuenemann, C. Elschner, A. A. Levin, B. Rellinghaus, K. Leo, and M. Riede, *Org. Electron.* **12**, 435 (2011).
- ¹⁵W. Zeng, K. S. Yong, Z. M. Kam, F. Zhu, and Y. Li, *Appl. Phys. Lett.* **97**, 133304 (2010).
- ¹⁶J. W. Kim, H. J. Kim, H. H. Lee, T. Kim, and J. J. Kim, *Adv. Funct. Mater.* **21**, 2067 (2011).
- ¹⁷R. Pandey and R. J. Holmes, *Adv. Mater.* **22**, 5301 (2010).
- ¹⁸T. Kaji, M. Zhang, S. Nakao, K. Iketaki, K. Yokoyama, C. T. Tang, and M. Hiramoto, *Adv. Mater.* **23**, 3320 (2011).
- ¹⁹C. H. Cheng, J. Wang, G. T. Du, S. H. Shi, Z. J. Du, Z. Q. Fan, J. M. Bian, and M. S. Wang, *Appl. Phys. Lett.* **97**, 083305 (2010).
- ²⁰V. P. S. Perera and K. Tennakone, *Sol. Energy Mater. Sol. Cells* **79**, 249 (2003).
- ²¹A. R. Kumarasinghe, W. R. Flavell, A. G. Thomas, A. K. Mallick, D. Tsoutsou, C. Chatwin, S. Rayner, P. Kirkham, and S. Warren, *J. Chem. Phys.* **127**, 114703 (2007).
- ²²M. Hirade and C. Adachi, *Appl. Phys. Lett.* **99**, 153302 (2011).
- ²³L. F. Drummy, R. J. Davis, D. L. Moore, M. Durstock, R. A. Vaia, and J. W. P. Hsu, *Chem. Mater.* **23**, 907 (2011).
- ²⁴A. Herzing, L. J. Richter, and I. M. Anderson, *J. Phys. Chem. C* **114**, 17501 (2010).
- ²⁵W. Schindler, M. Wollgarten, and K. Fostiropoulos, *Org. Electron.* **13**, 1100 (2012).
- ²⁶J. Yang, F. Zhu, B. Yu, H. Wang, and D. Yan, *Appl. Phys. Lett.* **100**, 103305 (2012).
- ²⁷F. Yang, M. Shtein, and S. R. Forrest, *Nat. Mater.* **4**, 37 (2005).
- ²⁸P. Peumans, A. Yakimov, and S. R. Forrest, *J. Appl. Phys.* **93**, 3693 (2003).
- ²⁹L. A. A. Pettersson, L. S. Roman, and O. Inganäs, *J. Appl. Phys.* **86**, 487 (1999).

- ³⁰W. Chen, D. C. Qi, H. Huang, X. Gao, and A. T. S. Wee, *Adv. Funct. Mater.* **21**, 410 (2011).
- ³¹W. Chen, C. Huang, X. Y. Gao, L. Wang, C. G. Zhen, D. C. Qi, S. Chen, H. L. Zhang, K. P. Loh, and Z. K. Chen, *J. Phys. Chem. B* **110**, 26075 (2006).
- ³²W. Chen, H. Huang, S. Chen, L. Chen, H. L. Zhang, X. Y. Gao, and A. T. S. Wee, *Appl. Phys. Lett.* **91**, 114102 (2007).
- ³³H. Huang, Y. Huang, J. Pflaum, A. T. S. Wee, W. Chen, and *Appl. Phys. Lett.* **95**, 263309 (2009).
- ³⁴T. Sakurai, T. Ohashi, H. Kitazume, M. Kubota, T. Suemasu, and K. Akimoto, *Org. Electron.* **12**, 966 (2011).

Table I. The performances of ZnPc (20 nm)/ZnPc:C₆₀ (40 nm)/C₆₀ (40 nm) photovoltaic cells with different buffer layers, which were measured under an AM 1.5G illumination.

	PCE (%)	V_{oc} (V)	J_{sc} (mA/cm ²)	FF
Bare ITO	2.38	0.54	9.68	0.46
ITO/CuI	3.19	0.52	10.3	0.59
ITO/PEDOT:PSS	1.55	0.55	9.01	0.32
ITO/PEDOT:PSS/CuI	4.56	0.51	15.1	0.59
ITO/PEDOT:PSS/CuI ^{a)}	4.37	0.53	14.8	0.56

^{a)}The cell structure is ZnPc (20 nm)/ZnPc:C₆₀ (20 nm)/C₆₀ (40 nm).

Captions of Figures

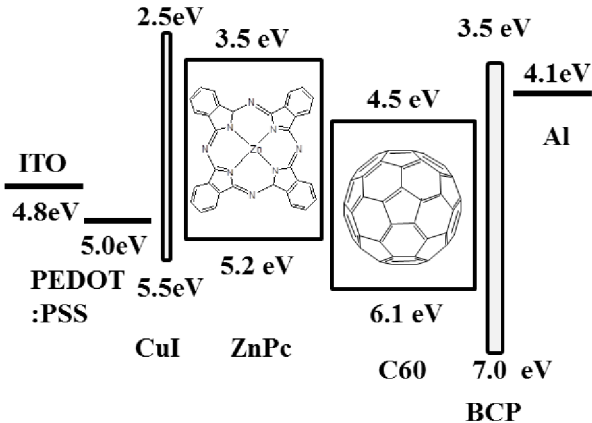
FIG. 1 Schematic energy level diagram of the OPV cell.

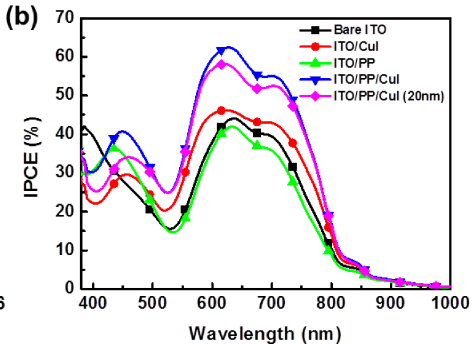
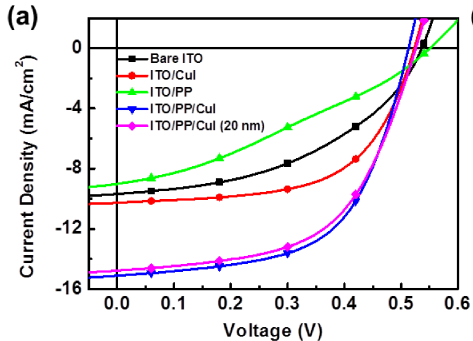
FIG. 2. (a) Current density versus voltage (J - V) characteristics and (b) incident photon to electron conversion efficiency (IPCE) for ZnPc (20 nm)/ZnPc:C₆₀ (40 nm)/C₆₀ (40 nm) organic photovoltaic cells fabricated on bare ITO, ITO/CuI, ITO/PEDOT:PSS (PP) and ITO/PEDOT:PSS/CuI (here, cell with 20 nm ZnPc:C₆₀ blend layer was also fabricated).

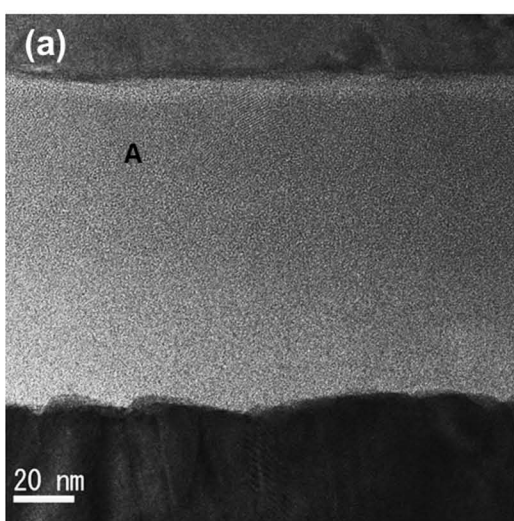
FIG. 3. (a) Bright field transmission electron microscopy (BFTEM) image and (b) energy filter transmission electron microscopy (EFTEM) image of the cell on ITO/PEDOT:PSS (PCE=1.55%). (c) BFTEM image and (d) EFTEM image of the cell on ITO/PEDOT:PSS/CuI (PCE=4.56%). (e) Large-scale images of the areas labelled with A in (a) and B, C, D in (c). Scale bar: 10 nm.

FIG. 4. AFM height images of 20 nm ZnPc films grown on (a) ITO/CuI, (b) ITO/PEDOT:PSS and (c) ITO/PEDOT:PSS/CuI. AFM phase images of them are given in (d), (e) and (c), respectively.

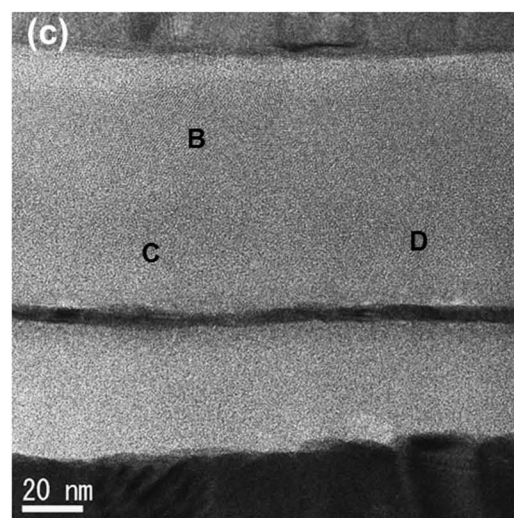
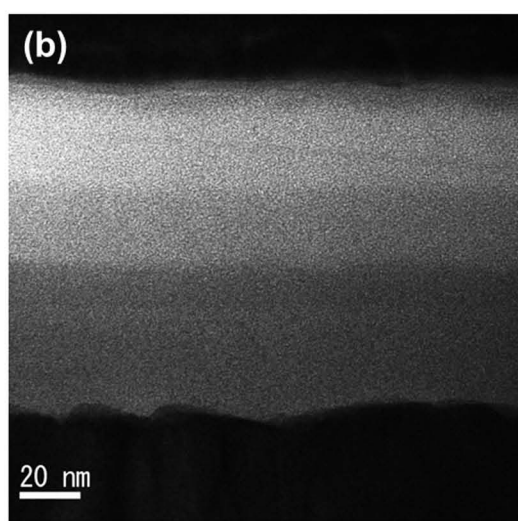
FIG. 5. X-ray diffraction of ZnPc films grown on bare ITO, ITO/CuI, ITO/PEDOT:PSS and ITO/PEDOT:PSS/CuI. The film thickness is about 40 nm when grown on ITO and ITO/CuI, 20 nm when grown on ITO/PEDOT:PSS and ITO/PEDOT:PSS/CuI.



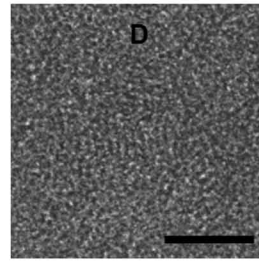
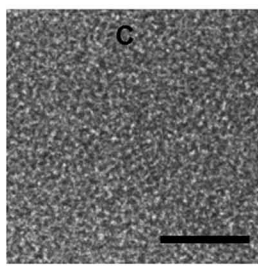
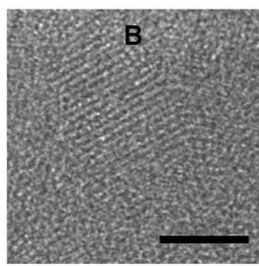
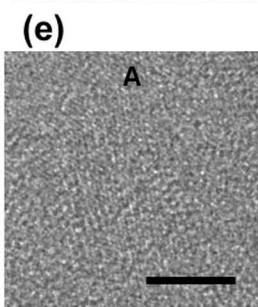
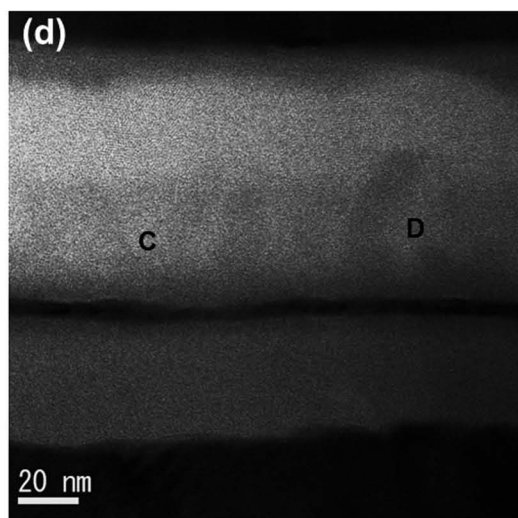


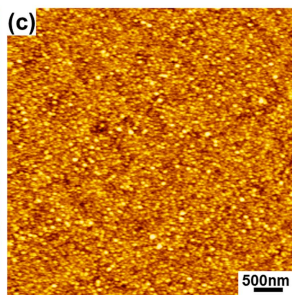
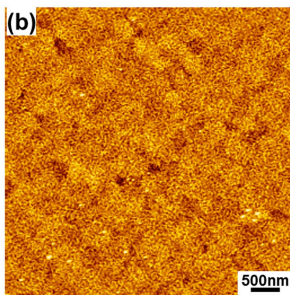
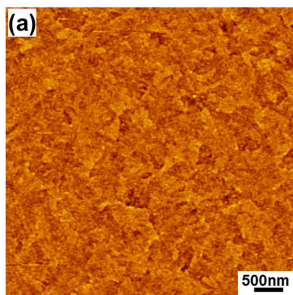


Al
BCP
C60
ZnPc:C60
ZnPc
PEDOT:PSS
ITO

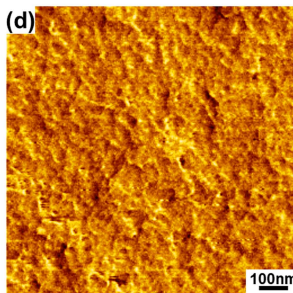


Al
BCP
C60
ZnPc:C60
ZnPc
CuI
PEDOT:PSS
ITO

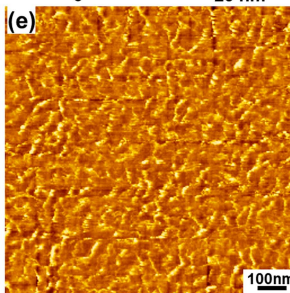




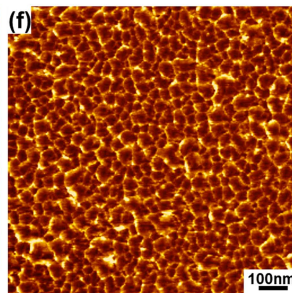
0 25 nm



0° 5°



0° 15°



0° 25°

